Lithiation-Induced Embrittlement of Multiwalled Carbon Nanotubes

Yang Liu,[†] He Zheng,[‡,#] Xiao Hua Liu,[†] Shan Huang,[§] Ting Zhu,[§,*] Jiangwei Wang,[‡] Akihiro Kushima,[⊥] Nicholas S. Hudak,[†] Xu Huang,[‖] Sulin Zhang,[‖] Scott X. Mao,[‡] Xiaofeng Qian,[¶] Ju Li,[⊥] and Jian Yu Huang[†,*]

[†]Center for Integrated Nanotechnologies, Sandia National Laboratories, Albuquerque, New Mexico 87185, United States, [‡]Department of Mechanical Engineering and Materials Science, University of Pittsburgh, Pittsburgh, Pennsylvania 15261, United States, [§]Woodruff School of Mechanical Engineering, Georgia Institute of Technology, Atlanta, Georgia 30332, United States, [⊥]Department of Materials Science and Engineering, University of Pennsylvania, Philadelphia, Pennsylvania 19104, United States, [‖]Department of Engineering Science and Mechanics, Pennsylvania State University, University Park, Pennsylvania 16802, United States, [¶]Department of Materials Science and Engineering, Massachusetts Institute of Technology, Cambridge, Massachusetts 02139, United States, and [#]School of Physics and Technology, Center for Electron Microscopy and MOE Key Laboratory of Artificial Micro- and Nano-structures, Wuhan University, Wuhan 430072, China

ABSTRACT Lithiation of individual multiwalled carbon nanotubes (MWCNTs) was conducted *in situ* inside a transmission electron microscope. Upon lithiation, the intertube spacing increased from 3.4 to 3.6 Å, corresponding to about 5.9% radial and circumferential expansions and ∼50 GPa tensile hoop stress on the outermost tube wall. The straight tube walls became distorted after lithiation. *In situ* compression and tension tests show that the lithiated MWCNTs were brittle with sharp fracture edges. Such a failure mode is in stark contrast with that of the pristine MWCNTs which are extremely flexible and fail in a "sword-in-sheath" manner upon tension. The lithiation-induced embrittlement is attributed to the mechanical effect of a "point-force" action posed by the intertubular lithium that induces the stretch of carbon—carbon bonds in addition to that by applied strain, as well as the chemical effect of electron transfer from lithium to the antibonding π orbital that weakens the carbon—carbon bond. The combined mechanical and chemical weakening leads to a considerable decrease of the fracture strain in lithiated MWCNTs. Our results provide direct evidence and understanding of the degradation mechanism of carbonaceous anodes in lithium ion batteries.

KEYWORDS: carbon nanotubes · lithiation embrittlement · lithium ion batteries · lattice expansion · brittle fracture

Due to their unique structures and physical properties, carbon nanotubes (CNTs) have attracted worldwide attention as a promising material for a wide range of applications, such as next generation electronics, optoelectronics, and biological and chemical applications.[1] The Young's modulus of arc-discharged CNTs was measured to be about 1 TPa, while the tensile strength was about 100 GPa,[2−6] and the Young's modulus obtained from chemical vapor deposition (CVD)-produced CNTs ranges from 3 GPa for CNTs with many defects to 600 GPa for CNTs with fewer defects,[7−9] indicating that the CNTs with less defects are extremely strong and mechanically robust.[10] CNTs also have high electrical conductivity; it has been reported that 50 nm long single-walled carbon nanotubes (SWCNTs) can carry an electric current density of about 4×10^9 A/cm^2.[11] Because of these excellent physical properties, CNTs are being extensively studied as a promising anode material for Li-ion batteries (LIBs).[12−21] For example, reversible capacities of SWCNTs and multiwalled carbon nanotube (MWCNTs) were reported to be 450−600 mAh/g[13,15] and up to 1000 mAh/g,[14] respectively, which are much higher than that of the commonly used anode material of graphite, 372 mAh/g. Furthermore, it is expected that a CNT anode should have a much longer cycle lifetime than the conventional carbonaceous anode due to the superior mechanical properties of the former. In addition, CNTs have been used as additives or compounded with other active materials, serving as conducting channels and expansion absorbers,[22−30] and they were also used in free-standing electrodes, acting as both the active materials and current collectors.[31−33]

The insertion/extraction of a large amount of lithium can induce the mechanical stress and failure in the electrodes, leading to the capacity fading of LIBs.[34,35] The promising application of CNTs in LIBs is due to their mechanical flexibility and robustness for retaining the electrical conducting channel and releasing the stress generated in the electrodes. Therefore, the mechanical properties of lithiated CNTs, which can present an important factor limiting the capacity and cyclability in LIBs, are critically important. Masarapu *et al.* reported that CNTs were broken into smaller pieces after 2000 cycles.[36] Similar fractures of CNTs were also observed recently after 200 cycles by Pol *et al.*[37] However, the mechanisms of lithiation-induced fracture in CNTs remain poorly understood. Here, we report an *in situ* transmission electron microscope (TEM) study of electrochemical lithiation of MWCNTs. Our results revealed the dramatic embrittlement of MWCNTs
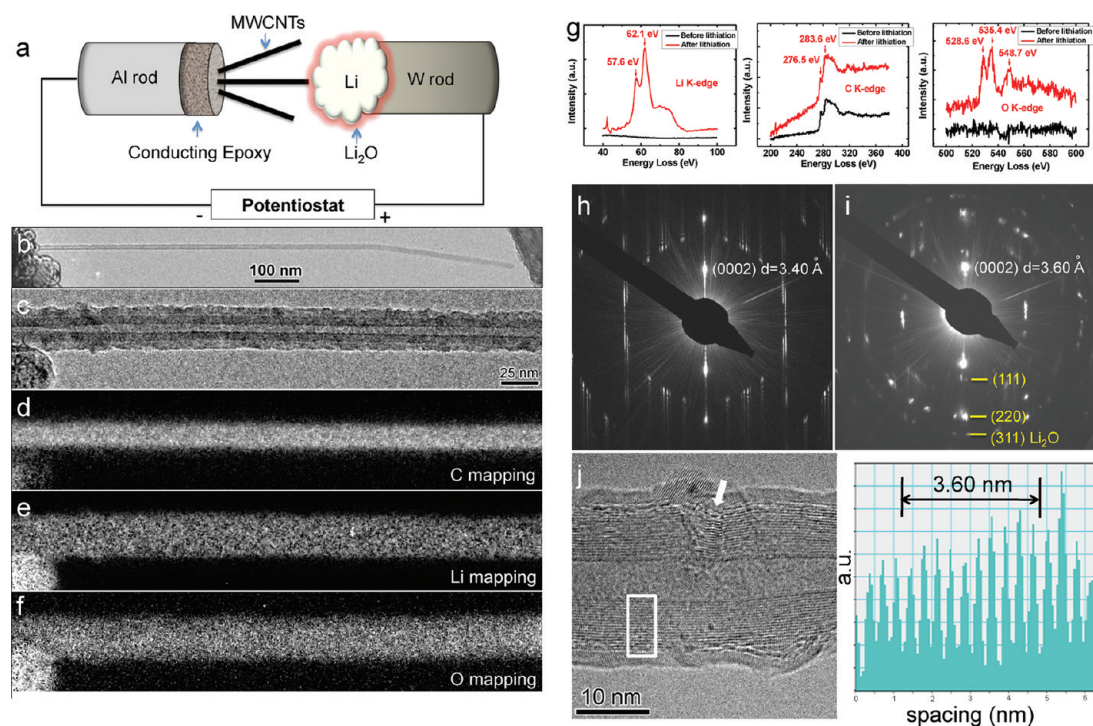
Figure 1. Lithiation of an arc-discharged MWCNT. (a) Schematic illustration of the *in situ* experimental setup. The MWCNTs were glued to an Al rod using conducting epoxy, serving as working electrode. Bulk lithium metal was scratched with a tungsten wire inside a glovebox and loaded into TEM with exposure time to the air less than 2 s, which served as counter/reference electrode. The naturally grown Li_2O layer on the surface of Li metal served as the solid electrolyte. The Li_2O/Li electrode was driven to contact one of the MWCNT electrodes *via* the piezoceramic controlled manipulator. Once the contact was established, a potential of -2 V was applied to the MWCNT with respect to the Li counter electrode to initiate the lithiation. **(b)** Pristine MWCNT with a diameter of about 15 nm before contacting the Li_2O/Li electrode. **(c)** Lithiated MWCNT showing a uniform Li_2O layer coated on the surface. **(d–f)** EELS maps of carbon, lithium, and oxygen, respectively, indicating that the lithiated MWCNT was coated with a uniform layer of Li_2O and the nanotube was lithiated. **(g)** EELS spectra of Li K-edge, C K-edge, and O K-edge before and after lithiation with the pre-edge background subtracted, showing the presence of lithium in the lithiated MWCNT. EDP before **(h)** and after **(i)** lithiation. The *d* spacing of the (0002) plane was increased from 3.40 to 3.60 Å after lithiation, indicating a 5.9% lattice expansion induced by lithiation. Note that the EDP (i) from the lithiated MWCNT also showed the polycrystal Li_2O diffraction pattern superimposed on the EDP from the MWCNT. **(j)** High-resolution TEM image of a lithiated MWCNT with an interlayer spacing of 3.60 Å, supporting the idea that lithium had indeed inserted into the intertubular gaps. The side walls became distorted as pointed by the white arrowhead.

during lithiation, which is attributed to the lithiation-induced chemo-mechanical weakening effects.

RESULTS AND DISCUSSION

We created an electrochemical device consisting of an individual MWCNT anode, a layer of Li_2O solid electrolyte, and a bulk Li metal cathode inside a TEM, which enables real-time observation of the structure evolution of electrodes during electrochemical reaction. Figure 1a shows the schematic illustration of our experimental setup. Experimental details are provided in the Methods section. Figure 1b shows a pristine MWCNT synthesized by arc-discharge with a diameter of about 15 nm before contacting the Li_2O/Li electrode. A few seconds after the MWCNT contacted the Li_2O layer, lithiation started. After a few minutes, the surface of the MWCNT was coated with a uniform layer of material with a thickness of about several nanometers (Figure 1c). The coating layer was proven to be Li_2O (Figure 1e–i). It is well-known that the capacity of CNT-based LIBs is reduced greatly in the first cycle, which has been attributed

to irreversible processes, such as formation of the solid electrolyte interface (SEI) layer.[16–18,38] The thin layer we observed here is related to the formation of the SEI layer on the surface of CNTs. After delithiation, this layer still existed, indicating a loss of capacity in the first cycle. It is interesting to note that such an SEI layer formed in all of the lithiated MWCNTs, but it was not obvious in other materials such as Si,[39] SnO_2,[40,41] and boron nitride (BN). Figure S1 in the Supporting Information shows the morphology evolution of a single BN nanotube under similar lithiation conditions as MWCNTs. Compared with the lithiation of MWCNTs (Figure 1 and Figure S2), no surface layer formed on the BN nanotube and the morphology did not change either, implying that the BN nanotube could not be lithiated under the similar lithiation condition as that of MWCNT, because the BN is not electrically conducting. Electron energy loss spectroscopy (EELS) maps of carbon, lithium, and oxygen in the MWCNT are shown in Figure 1d–f, respectively. The EELS map of carbon showed smaller diameter than that of Li and O, indicating that the lithiated MWCNT was coated

with a uniform layer of Li_2O. Furthermore, the uniform contrast of the Li map indicated that the nanotube shells were lithiated. Figure 1g presents the EELS spectra from pristine (black curve) and lithiated MWCNTs (red curve). The rise of Li K-edge peaks at 57.6 and 62.1 eV and O K-edge peaks with an onset about 525 eV from the MWCNT after lithiation confirmed the presence of lithium in the lithiated MWCNT and supported the existence of Li_2O on the surface. From the electron diffraction pattern (EDP) before (Figure 1h) and after (Figure 1i) lithiation, the spacing of the (0002) plane was increased from 3.40 to 3.60 Å. Similar interlayer expansion was also observed using X-ray diffraction (XRD) technique.[16] Unlike a free-standing graphite (stack of flat graphenes), in which interlayer expansions can be accommodated by free out-of-plane motion of graphene layers to maintain a stress-free condition, the 5.9% interlayer expansion induced by lithium insertion on the closed-shell geometry of the MWCNT will have serious consequences on the internal stress state. Since a circumferential strain of equal magnitude must accompany the radial expansion, a tensile hoop stress of ~50 GPa was generated on the outmost tube of the MWCNT (compared to near zero stress in a piece of lithiated but free-standing graphite), even before any external load is applied to the MWCNT.

The diffraction rings superimposed on the EDP from the lithiated MWCNT (Figure 1i) could be indexed as polycrystalline Li_2O, which further proves the existence of Li_2O in the lithiated MWCNT. High-resolution TEM (HRTEM) image of a lithiated MWCNT (Figure 1j) with an interlayer spacing of 3.60 Å confirms that lithium had indeed inserted into the intertubular gaps. It is noteworthy that the side walls became distorted after lithiation, as pointed by the white arrowhead in Figure 1j.

We have tested the mechanical properties of lithiated MWCNTs using the piezomanipulator to push and pull the MWCNTs. Figure 2a–d and movie S1 of the Supporting Information show the structural evolution of a MWCNT when it was bent with increasing curvature. The sharp obtuse angle developed at its bend (Figure 2c, as pointed by the white arrowhead). This lithiated MWCNT fractured as we pulled back the piezomanipulator (Figure 2d). The sharp fracture edge is strikingly different from the "sword-in-sheath" failure mode of pristine MWCNTs,[3,5] indicating the brittle fracture of lithiated MWCNTs. This radically different fracture mode is rather surprising, considering that pristine arc-discharged MWCNTs are extremely flexible and large bending deformation can be fully recovered after unloading.[2−6]

Obviously, the embrittlement of MWCNTs was related to lithium insertion. It is well-known that lithium ions can enter tubes through surface defects or open ends.[42,43] Chemical vapor deposition (CVD)-produced CNTs generally have more defects than arc-discharge-produced CNTs. This implies that the lithium ion can penetrate the walls of the former much easier than
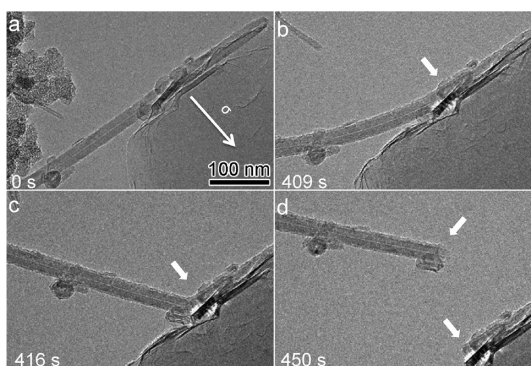

Figure 2. Brittle fracture of a lithiated arc-discharged MWCNT. (a–d) Time-lapse TEM images showing the structure evolution of a lithiated MWCNT under compression and tension. (a) Lithiated MWCNT side-contacted with Li_2O/Li electrode. (b) MWCNT was lithiated and bent. (c) MWCNT was further compressed. The sharp obtuse angle shape of the bent MWCNT indicated that plastic deformation occurred at the bent point (as pointed by the white arrowhead), instead of undergoing buckling. (d) Brittle fracture of the lithiated MWCNT under tension. The shape of the fracture edges is pointed out by the white arrowheads.
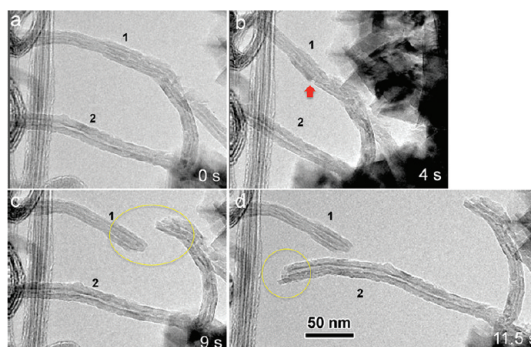

Figure 3. Brittle fracture of a lithiated CVD–MWCNT. (a–d) Structure evolution of a lithiated MWCNT when it was pressed and pulled. (a) Lithiated MWCNT including two segments as marked by "1" and "2". (b) Tiny crack was initiated in the side walls (as pointed by the red arrowhead) while the MWCNT was compressed. (c) Brittle fracture of segment 1 while the MWCNT was pulled back to its original position. (d) Brittle fracture of segment 2 of the MWCNT.

the latter. Chemical etching[19,20] and mechanical ball-milling[15,18] were used to introduce more defects into CNTs to increase the capacities. Therefore, it is also worth investigating the mechanical properties of CVD-produced CNTs after lithiation. Figure 3 shows the structural evolution of a lithiated CVD–MWCNT under compression and tension tests. A bent CVD–MWCNT including two segments (marked by "1" and "2" in Figure 3) after lithiation is shown in Figure 3a. It is clear that the surface of the lithiated MWCNT was coated with a Li_2O layer with polycrystal contrast. A tiny crack on the side walls was initiated (as pointed by the red arrowhead in Figure 3b) during compression of the MWCNT (Figure 3b). Brittle fracture occurred to segment 1 when the MWCNT was pulled back to its original position (Figure 3c), and segment 2 also underwent brittle fracture while the MWCNT was further
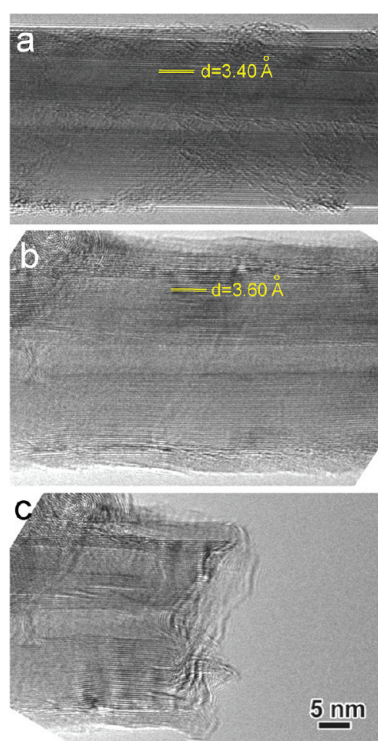
Figure 4. Brittle fracture of a lithiated arc-discharged MWCNT without electron beam illumination during mechanical deformation. (a) High-resolution TEM image of a MWCNT before lithiation, showing the interlayer spacing was about 3.40 Å. (b) High-resolution TEM image of the MWCNT after lithiation, demonstrating the interlayer spacing was increased to 3.60 Å, indicating a 5.9% lattice expansion induced by lithiation. (c) High-resolution TEM image of the fracture edge. All of the lithiation experiments and mechanical tests were performed with beam blank.

Figure 5. Brittle fracture of CVD−MWCNTs after 100 cycles in a Swagelok cell. (a−d) Time-lapse TEM images showing the structure evolution of a MWCNT after 100 cycles. (a) A 100 times cycled MWCNT with one end immersed in a bundle of MWCNTs and the other end fixed to a tungsten tip using electron-beam-induced deposition (EBID) of amorphous carbon. (b,c) Curvature increased as the tungsten tip was continuously driven forward. (d) Brittle fracture of the MWCNT with a sharp edge under compression.

pulled back (Figure 3d). Again, as the phenomena observed in the arc-discharged MWCNT, the fracture surface is sharp, and no "sword-in-sheath" failure was observed. Similar brittle fracture was observed in CVD−MWCNTs after multicycling.[36,37]

Although the dose as less as possible was used to capture the images and videos in the above experiments, electron beam irradiation with sufficient dose could introduce interlayer defects in MWCNTs, thus reducing their modulus and strength.[44−48] In order to assess the effects of electron beam irradiation in our experiments, we also conducted lithiation and mechanical tests under the beam-blank condition. Figure 4a is the HRTEM image of a pristine arc-discharged MWCNT, showing a straight tube with a clean surface and a uniform hollow structure. The interlayer spacing was also about 3.40 Å, which is consistent with that of MWCNT from previous EDP measurement (Figure 1h). After lithiation, the side walls became distorted and the interlayer spacing was increased to 3.60 Å (Figure 4b), corresponding to about 5.9% lattice expansion induced by lithium insertion. The MWCNT broke with sharp fracture edges (Figure 4c) under slight shake induced by opening the valve of TEM in blanking beam
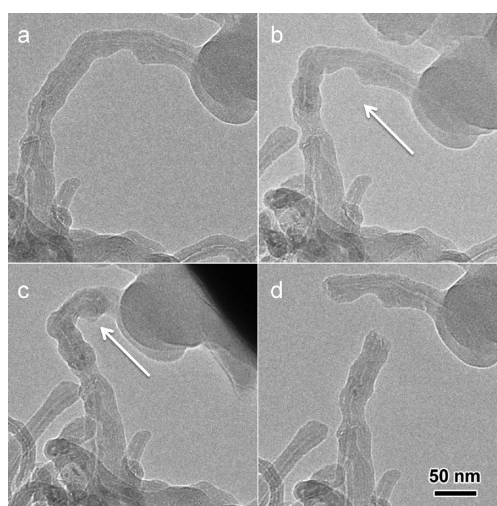
test. These results further confirmed the brittleness of lithiated CNTs.

Besides the *in situ* lithiation experiments, we also conducted *ex situ* multiple cycling of CVD−MWCNTs in a Swagelok-type cell using the MWCNT as the working electrode, 1 M LiPF$_6$ in ethylene carbonate and dimethyl carbonate (EC/DMC, 2:1 by volume) as the electrolyte, and Li metal as the counter electrode. After the MWCNTs were cycled 100 times, they were transferred into the TEM from the glovebox using a sealed bag filled with dry helium with exposure time to the air less than 2 s and used for mechanical tests. Figure 5a shows a cycled MWCNT with one end immersed in a bundle of MWCNTs and the other end fixed to a tungsten tip using electron-beam-induced deposition (EBID) of amorphous carbon. The surface of the MWCNT was coated with an SEI layer after electrochemical cycling. The structure evolution of the cycled MWCNT under compression is shown in Figure 5b−d. The MWCNTs broke with sharp fracture edges (Figure 5d), as similarly observed during *in situ* fracture tests of lithiated MWCNTs. This mechanical test with cycled MWCNTs from a conventional electrochemical cell confirmed the lithiation-induced embrittlement of MWCNTs. To compare the mechanical behavior of the lithiated MWCNTs, mechanical tests of pristine arc-discharged MWCNTs used in this work were carried out, as shown in Figure 6a−f and movie S2 in the Supporting Information. Figure 6a shows a pristine arc-discharged MWCNT with one end glued to the substrate using conducting epoxy and the other end fixed to a tungsten tip using EBID of amorphous carbon. Tungsten tip
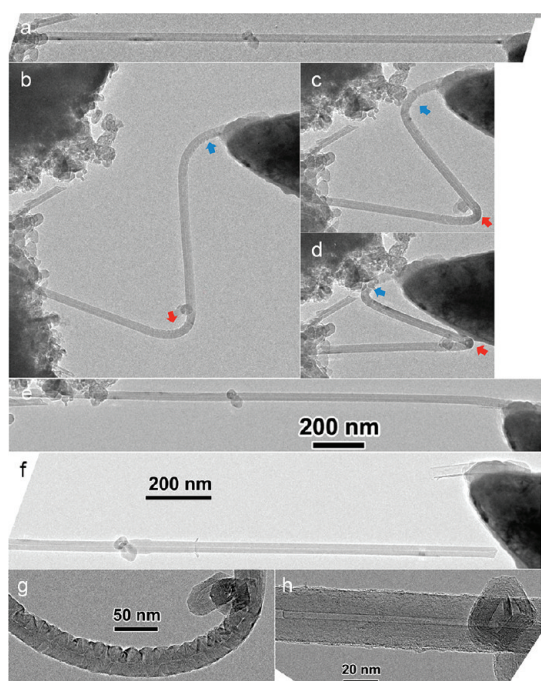
Figure 6. Compression and tension tests of pristine arc-discharged MWCNTs. (a–f) Structure evolution of a pristine MWCNT under compressive and tensile load. (a) Pristine arc-discharged MWCNT with one end glued to the substrate using conducting epoxy and the other end fixed to a tungsten tip using EBID of amorphous carbon. (b) Bent MWCNT showing "S" shape and buckling on the compression side of the nanotubes (as pointed by the red and blue arrowheads). (c) Increase of bent angle on the MWCNT. (d) MWCNT buckled as the tungsten tip was continuously driven forward. (e) MWCNT fully recovered to its original straight shape without any obvious structural damage after compression and tension. (f) Few outmost walls peeling off at the end of the MWCNT as the tungsten tip was extracted, showing the "sword-in-sheath" failure. (g) Zoom-in TEM image at the buckling area showing the ripple-like distortion of the graphene walls. (h) Full recovery of the buckling area in Figure 6g after several sequences of compression and tension.

was driven forward to compress and bend the MWCNT *via* the piezomanipulator (Figure 6b–d). The MWCNT was bent to "S" shape, and buckling-induced ripples formed on the compressed side of nanotubes (Figure 6b), as pointed by the red and blue arrowheads. The zoom-in TEM image at the buckled area (Figure 6g) shows the ripple-like distortion of tube walls. The bend angle became larger (Figure 6c), and the MWCNT was bent over itself (Figure 6d) as the tungsten tip continuously drove forward. After being pressed, the tungsten tip was extracted to the original position, and the MWCNT recovered its original straight shape (Figure 6e). This procedure can be repeated over and over again, without causing any obvious structural damage to the nanotubes. The buckled area shown in Figure 6g was straightened out and fully recovered after several rounds of pushing and pulling (Figure 6h). After the bending test, the tungsten tip was further extracted to carry out the tensile test. A few outmost walls were peeled off at the end of the MWCNT (Figure 6f), showing the "sword-in-sheath" failure

phenomena, which is different from the formation of sharp edges after brittle fracture of lithiated MWCNTs. These bending and pulling tests prove that the pristine MWCNTs are strong and flexible and can undergo reversible deformation in bending and pressing, consistent with the results from other groups.[3,5,6]

The above experiments indicate that the embrittlement of MWCNTs is closely related to lithium insertion. When lithium enters the tubes from either the surface defects or open ends, it diffuses between the tube walls and interacts with neighboring carbon atoms.[42] To evaluate the embrittlement effects of lithium, we performed the molecular orbital (MO) theory calculations using the AM1 method[49] (see the Modeling section). In the absence of the axial load, MO simulations of a double-walled CNT well captured the radial expansion due to lithium insertion between the tube walls (Figure 7a, 5.9% intertube expansion from experiment *versus* 6.4% from simulation). Further MO simulations of the axially strained CNTs revealed both the mechanical and chemical effects of embrittlement by lithium. To assess the mechanical weakening, we note that the axial tensile strain causes radial contraction of the CNT. As a result, the intertubular lithium is squeezed by the tube walls and it, in turn, acts effectively as a local point force pushing against them (Figure 7b). Such squeezing and associated "point-force" effects arise because of the finite curvature of the tube walls and are expected to become insignificant in planar graphene and layered graphite.[50,51] At low loads, the pushing force induces the extended bending deformation in cylindrical tubes. As the applied axial tension increases, the localized deformation will gradually take over,[52,53] causing large elongation of the C–C bonds adjacent to lithium. Such bond stretch is additional to that induced by the applied mechanical load. For instance, at 15% axial strain, the C–C bond near lithium (pink lines in Figure 7b) is elongated to 1.59 Å, as opposed to 1.54 Å in the pristine counterpart. The additional bond stretch increases with the axial load and thus lowers the applied strain necessary to fracture the CNT. This effect represents the mechanical weakening caused by lithium insertion.

On the other hand, the chemical weakening was assessed in terms of charge transfer from lithium to carbon. Figure 7c shows the charge contour of a double-walled CNT subject to 15% applied strain. In this case, lithium loses electron and becomes positively charged (+0.55e, not shown as it is outside the range of the color bar), while adjacent carbon atoms gain electrons that are expected to fill the antibonding π orbitals of C–C bonds, thus inducing the chemical weakening.[54] The charge increase is, however, limited in these carbon atoms, since the 0.55e charge transferred from one lithium has to be shared by several carbon atoms. In addition, compared to the zero-strained CNT, further change of charges in these
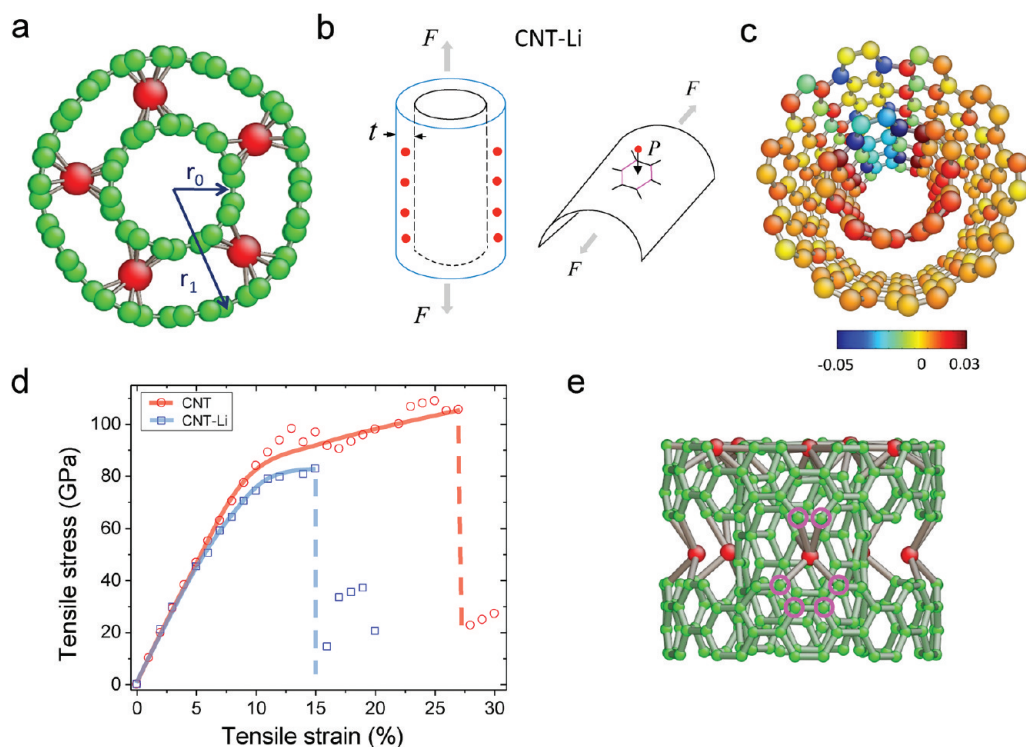
Figure 7. Molecular orbital theory modeling of lithium embrittlement of a double-walled CNT. (a) Radial expansion caused by insertion of intertubular lithium when the applied axial strain is zero: $r_0 = 3.42$ Å, $r_1 = 6.85$ Å without lithium, and $r_0 = 3.38$ Å, $r_1 = 7.03$ Å with lithium, giving the intertube expansion of 6.4%. Carbon atoms are green and lithium red. (b) Schematic illustrations: (left) intertubular lithium is squeezed by the tube walls due to the decreasing intertubular spacing t with increasing axial force F; (right) in response to squeezing, intertubular lithium pushes against the tube walls, as represented by a force P acting on the tube, causing additional deformation of the adjacent C—C bonds. (c) Mulliken charges induced by insertion of intertubular lithium. In this case, only one column of lithium is inserted along the axial direction, in order to increase the color contrast for highlighting the charge changes in carbon atoms. The lithium atom is positively charged, but not shown as its charge ($+0.55e$) is outside the range of color bar. (d) Stress *versus* strain (symbols) of an axially strained tube with and without intertubular lithium; solid lines are the fitting curves. (e) Atomic structure of a fractured double-walled CNT; pink circles indicate the carbon atoms that originally belong to a six-membered ring, which is broken due to the combined effects of applied axial load and lithium embrittlement.

carbon atoms is negligibly small with increasing axial strain. Furthermore, MO calculations at 0 K give about 14% athermal strain of fracture in a lithiated double-walled CNT (Figure 7d,e), as opposed to 27% in the pristine counterpart. In the latter case, the drastic change of the tube stiffness in the stress—strain responses (the line in orange in Figure 7d) can be attributed to the transition from both the stretch and rotation of C—C bonds at small strains to the dominant deformation mode of stretch of C—C bonds at large strains. Interestingly, fracture of the lithiated tubes occurs around such transition point, implying that the inserted lithium compromises the stretching capability of C—C bonds, thereby causing a considerable reduction of fracture strain. It should be noted that the lithiation-induced decrease of the bond strain of fracture could also have a valve effect[55] on suppressing the energy-dissipative irreversible deformation, such as formation and evolution of the Stone—Wales defects,[56] thereby leading to the apparent brittle fracture in lithiated CNTs.

Finally, we note that the above simplified model of a double-walled CNT allowed us to capture the fundamental embrittlement effect of interlayer Li in terms of

the mechanical weakening *via* a "point-force" effect and chemical weakening of C—C bonds *via* charge transfer from lithium to carbon, while the intrinsic defects can decrease the mechanical strength and bending modulus of CNTs due to the break of quasi-one-dimensional atomic structure. In the future, the more accurate density functional theory study should be performed to assess the accuracy of the present molecular orbital theory calculations, and systematic modeling studies are needed for understanding the strength controlling dynamics of defect evolution and progressive fracture that could involve the surface initiation and inward propagation of cracks in lithiated MWCNTs.

CONCLUSION

In summary, lithiation of the individual MWCNTs was realized by *in situ* TEM experiments. Upon lithiation, a uniform layer of Li$_2$O was coated on the tube surface, which is related to the SEI layer formation and contributes to the large irreversible capacities in the first cycle. The interlayer spacing increased from an equilibrium value of 3.4 to 3.6 Å, indicating about 5.9% radial and circumferential expansions and ~50 GPa tensile hoop stress.

The lithiated MWCNTs are brittle with sharp fracture surface upon mechanical loading, which is in sharp contrast to the high flexibility and the "sword-in-sheath" fracture of pristine MWCNTs. Quantum chemical modeling indicated that the lithiation-induced embrittlement can be attributed to the combined effects of mechanical and chemical weakening of C−C bonds by lithium insertion, as well as the tensile hoop prestress.

METHODS

***In Situ* TEM Setup.** A few MWCNTs were glued to an Al rod using conducting epoxy, serving as the working electrode. Bulk lithium metal was scratched with a tungsten wire inside a glovebox, and the W wire with Li attached in the end was loaded into the TEM using a sealed bag filled with dry helium, which served as the counter/reference electrode. The exposure time to the air was estimated to be less than 2 s. The naturally grown Li_2O layer on the surface of Li metal served as the solid electrolyte for Li^+ transport. The Li_2O/Li electrode side was driven to contact one of the MWCNT electrodes *via* a piezo-manipulator (Nanofactory TEM-Scanning Tunneling Microscopy (STM) holder). Once a contact was established, a potential of −2 V was applied to the MWCNT with respect to the Li counter electrode to initiate the lithiation. After lithiation, the MWCNTs were pushed and pulled against the Li_2O surface to test their mechanical response. The experiments were performed at room temperature inside a Tecnai F30 high-resolution TEM under 100 kV imaging. The irradiation doses on the MWCNTs in all of the experiments were much less than that which could generate a large number of defects and damage the MWCNTs.

***Ex Situ* Swagelok-Type Cell.** Lithium half-cells for *ex situ* testing were assembled in Swagelok-type fixtures in the dry glovebox. The cells consisted of a working electrode (MWCNT on copper substrate), glass microfiber separators (Whatman GF/D) soaked with electrolyte solution, and a lithium foil counter/reference electrode (FMC Lithium). The electrolyte solution was 1 M $LiPF_6$ in a 2:1 mixture (by volume) of ethylene carbonate and dimethyl carbonate (Novolyte). Galvanostatic cycling was performed on the cells at room temperature with a PAR 273A potentiostat/galvanostat. The cycling current was 370 mA/g, and voltage limits were 10 mV and 2.0 V.

Modeling. To evaluate the lithium embrittlement effect on CNTs, we have performed the molecular orbital theory calculations using the AM1 method,[49] implemented in the commercial package of MOPAC. We took a double-walled CNT with the equilibrium radius of the inner and outer tube being $r_0 = 3.42$ Å and $r_1 = 6.85$ Å, respectively. The longitudinal axis of the tube was oriented along the zigzag direction of the graphite sheet. There are 240 carbon atoms and 10 lithium atoms in the system. The intertubular lithium corresponds to a 2×2 in-plane ordering on the carbon honeycomb lattice.[50] As a result, there are five intertubular lithium atoms seen in the cross section (Figure 7a), and there is one intertubular lithium in every other ring along the longitudinal direction of the tube. Periodic boundary conditions were imposed along the axial direction of the tube. The stress−strain curves in Figure 7d were obtained by a series of energy minimizations at various prescribed axial strains. The stress was calculated by dividing the resultant axial force from MOPAC with the nominal cross sectional area $A = \pi[(r_1 + t)^2 - r_0^2]$, where t denotes the equilibrium intertube spacing taken as 3.4 Å. Young's modulus of the pristine DWCNT at 0% strain was calculated as 1007.4 GPa, consistent with the experimental measurement.[2]

REFERENCES AND NOTES

1. Dresselhaus, M. S.; Dresselhaus, G.; Avouris, P. *Carbon Nanotubes: Synthesis, Structure, Properties and Applications*; Springer-Verlag: Berlin, 2001.
2. Yu, M.-F.; Lourie, O.; Dyer, M. J.; Moloni, K.; Kelly, T. F.; Ruoff, R. S. Strength and Breaking Mechanism of Multiwalled Carbon Nanotubes under Tensile Load. *Science* **2000**, *287*, 637–640.
3. Demczyk, B. G.; Wang, Y. M.; Cumings, J.; Hetman, M.; Han, W.; Zettl, A.; Ritchie, R. O. Direct Mechanical Measurement of the Tensile Strength and Elastic Modulus of Multiwalled Carbon Nanotubes. *Mater. Sci. Eng.* **2002**, *A334*, 173–178.
4. Thostenson, E. T.; Ren, Z.; Chou, T.-W. Advances in the Science and Technology of Carbon Nanotubes and Their Composites: A Review. *Compos. Sci. Technol.* **2001**, *61*, 1899–1912.
5. Coleman, J. N.; Khan, U.; Blau, W. J.; Gun'ko, Y. Small but Strong: A Review of the Mechanical Properties of Carbon Nanotube−Polymer Composites. *Carbon* **2006**, *44*, 1624–1652.
6. Falvo, M. R.; Clary, G. J.; Taylor, R. M.; Chi, V.; Brooks, F. P.; Washburn, S.; Superfine, R. Bending and Buckling of Carbon Nanotubes under Large Strain. *Nature* **1997**, *389*, 582–584.
7. Gao, R.; Wang, Z. L.; Bai, Z.; de Heer, W. A.; Dai, L.; Gao, M. Nanomechanics of Individual Carbon Nanotubes from Pyrolytically Grown Arrays. *Phys. Rev. Lett.* **2000**, *85*, 622–625.
8. Salvetat, J.-P.; Kulik, A. J.; Bonard, J.-M.; Briggs, G. A. D.; Stöckli, T.; Méténier, K.; Bonnamy, S.; Béguin, F.; Burnham, N. A.; Forró, L. Elastic Modulus of Ordered and Disordered Multiwalled Carbon Nanotubes. *Adv. Mater.* **1999**, *11*, 161–165.
9. Wei, X.-L.; Liu, Y.; Chen, Q.; Wang, M.-S.; Peng, L.-M. The Very-Low Shear Modulus of Multi-walled Carbon Nanotubes Determined Simultaneously with the Axial Young's Modulus *via In Situ* Experiments. *Adv. Funct. Mater.* **2008**, *18*, 1555–1562.
10. Zhu, T.; Li, J. Ultra-strength Materials. *Prog. Mater. Sci.* **2010**, *55*, 710–757.
11. Javey, A.; Qi, P.; Wang, Q.; Dai, H. From the Cover: Ten- to 50-nm-Long Quasi-Ballistic Carbon Nanotube Devices

Obtained without Complex Lithography. *Proc. Natl. Acad. Sci. U.S.A.* **2004**, *101*, 13408–13410.

12. Wu, Y. P.; Rahm, E.; Holze, R. Carbon Anode Materials for Lithium Ion Batteries. *J. Power Sources* **2003**, *114*, 228–236.

13. Landi, B. J.; Ganter, M. J.; Cress, C. D.; DiLeo, R. A.; Raffaelle, R. P. Carbon Nanotubes for Lithium Ion Batteries. *Energy Environ. Sci.* **2009**, *2*, 638–654.

14. Lahiri, I.; Oh, S.-W.; Hwang, J. Y.; Cho, S.; Sun, Y.-K.; Banerjee, R.; Choi, W. High Capacity and Excellent Stability of Lithium Ion Battery Anode Using Interface-Controlled Binder-Free Multiwall Carbon Nanotubes Grown on Copper. *ACS Nano* **2010**, *4*, 3440–3446.

15. Gao, B.; Kleinhammes, A.; Tang, X. P.; Bower, C.; Fleming, L.; Wu, Y.; Zhou, O. Electrochemical Intercalation of Single-Walled Carbon Nanotubes with Lithium. *Chem. Phys. Lett.* **1999**, *307*, 153–157.

16. Eom, J. Y.; Kwon, H. S.; Liu, J.; Zhou, O. Lithium Insertion into Purified and Etched Multi-walled Carbon Nanotubes Synthesized on Supported Catalysts by Thermal CVD. *Carbon* **2004**, *42*, 2589–2596.

17. Chew, S. Y.; Ng, S. H.; Wang, J.; Novák, P.; Krumeich, F.; Chou, S. L.; Chen, J.; Liu, H. K. Flexible Free-Standing Carbon Nanotube Films for Model Lithium-Ion Batteries. *Carbon* **2009**, *47*, 2976–2983.

18. Gao, B.; Bower, C.; Lorentzen, J. D.; Fleming, L.; Kleinhammes, A.; Tang, X. P.; McNeil, L. E.; Wu, Y.; Zhou, O. Enhanced Saturation Lithium Composition in Ball-Milled Single-Walled Carbon Nanotubes. *Chem. Phys. Lett.* **2000**, *327*, 69–75.

19. Shimoda, H.; Gao, B.; Tang, X. P.; Kleinhammes, A.; Fleming, L.; Wu, Y.; Zhou, O. Lithium Intercalation into Etched Single-Wall Carbon Nanotubes. *Physica B* **2002**, *323*, 133–134.

20. Shimoda, H.; Gao, B.; Tang, X. P.; Kleinhammes, A.; Fleming, L.; Wu, Y.; Zhou, O. Lithium Intercalation into Opened Single-Wall Carbon Nanotubes: Storage Capacity and Electronic Properties. *Phys. Rev. Lett.* **2002**, *88*, 015502-1–4.

21. Lee, S. W.; Yabuuchi, N.; Gallant, B. M.; Chen, S.; Kim, B.-S.; Hammond, P. T.; Shao-Horn, Y. High-Power Lithium Batteries from Functionalized Carbon-Nanotube Electrodes. *Nat. Nanotechnol.* **2010**, *5*, 531–537.

22. Lee, S.-Y.; Park, J. H.; Park, P.; Kim, J. H.; Ahn, S.; Lee, K.-J.; Lee, H.-D.; Park, J.-S.; Kim, D.-H.; Jeong, Y. U. Effect of MWCNT on the Performances of the Rounded Shape Natural Graphite as Anode Material for Lithium-Ion Batteries. *J. Solid State Electrochem.* **2010**, *14*, 951–956.

23. Wu, F. D.; Wang, Y. Self-Assembled Echinus-like Nanostructures of Mesoporous CoO Nanorod@CNT for Lithium-Ion Batteries. *J. Mater. Chem.* **2011**, *21*, 6636–6641.

24. Goyal, A.; Reddy, A. L. M.; Ajayan, P. M. Flexible Carbon Nanotube–Cu$_2$O Hybrid Electrodes for Li-Ion Batteries. *Small* **2011**, *7*, 1709–1713.

25. Xu, C.; Sun, J.; Gao, L. Synthesis of Multiwalled Carbon Nanotubes That Are Both Filled and Coated by SnO$_2$ Nanoparticles and Their High Performance in Lithium-Ion Batteries. *J. Phys. Chem. C* **2009**, *113*, 20509–20513.

26. Wang, Y.; Zeng, H. C.; Lee, J. Y. Highly Reversible Lithium Storage in Porous SnO$_2$ Nanotubes with Coaxially Grown Carbon Nanotube Overlayers. *Adv. Mater.* **2006**, *18*, 645–649.

27. Wang, W.; Kumta, P. N. Reversible High Capacity Nanocomposite Anodes of Si/C/SWNTs for Rechargeable Li-Ion Batteries. *J. Power Sources* **2007**, *172*, 650–658.

28. Eom, J.-Y.; Kwon, H.-S. Preparation of Single-Walled Carbon Nanotube/Silicon Composites and Their Lithium Storage Properties. *ACS Appl. Mater. Interfaces* **2011**, *3*, 1015–1021.

29. Wang, Y.; Wu, M.; Jiao, Z.; Lee, J. Y. Sn@CNT and Sn@C@CNT Nanostructures for Superior Reversible Lithium Ion Storage. *Chem. Mater.* **2009**, *21*, 3210–3215.

30. Liu, C.; Li, F.; Ma, L.-P.; Cheng, H.-M. Advanced Materials for Energy Storage. *Adv. Mater.* **2010**, *22*, E28–E62.

31. Chen, J.; Minett, A. I.; Liu, Y.; Lynam, C.; Sherrell, P.; Wang, C.; Wallace, G. G. Direct Growth of Flexible Carbon Nanotube Electrodes. *Adv. Mater.* **2008**, *20*, 566–570.

32. Cui, L.-F.; Hu, L.; Choi, J. W.; Cui, Y. Light-Weight Free-Standing Carbon Nanotube–Silicon Films for Anodes of Lithium Ion Batteries. *ACS Nano* **2010**, *4*, 3671–3678.

33. Hu, L.; Wu, H.; La Mantia, F.; Yang, Y.; Cui, Y. Thin, Flexible Secondary Li-Ion Paper Batteries. *ACS Nano* **2010**, *4*, 5843–5848.

34. Li, H.; Wang, Z.; Chen, L.; Huang, X. Research on Advanced Materials for Li-Ion Batteries. *Adv. Mater.* **2009**, *21*, 4593–4607.

35. Kasavajjula, U.; Wang, C.; Appleby, A. J. Nano- and Bulk-Silicon-Based Insertion Anodes for Lithium-Ion Secondary Cells. *J. Power Sources* **2007**, *163*, 1003–1039.

36. Masarapu, C.; Subramanian, V.; Zhu, H.; Wei, B. Long-Cycle Electrochemical Behavior of Multiwall Carbon Nanotubes Synthesized on Stainless Steel in Li Ion Batteries. *Adv. Funct. Mater.* **2009**, *19*, 1008–1014.

37. Pol, V. G.; Thackeray, M. M. Spherical Carbon Particles and Carbon Nanotubes Prepared by Autogenic Reactions: Evaluation as Anodes in Lithium Electrochemical Cells. *Energy Environ. Sci.* **2011**, *4*, 1904–1912.

38. Kim, Y. A.; Kojima, M.; Muramatsu, H.; Umemoto, S.; Watanabe, T.; Yoshida, K.; Sato, K.; Ikeda, T.; Hayashi, T.; Endo, M.; *et al. In Situ* Raman Study on Single- and Double-Walled Carbon Nanotubes as a Function of Lithium Insertion. *Small* **2006**, *2*, 667–676.

39. Liu, X. H.; Zhang, L. Q.; Zhong, L.; Liu, Y.; Zheng, H.; Wang, J. W.; Cho, J.-H.; Dayeh, S. A.; Picraux, S. T.; Sullivan, J. P.; *et al.* Ultrafast Electrochemical Lithiation of Individual Si Nanowire Anodes. *Nano Lett.* **2011**, *11*, 2251–2258.

40. Huang, J. Y.; Zhong, L.; Wang, C. M.; Sullivan, J. P.; Xu, W.; Zhang, L. Q.; Mao, S. X.; Hudak, N. S.; Liu, X. H.; Subramanian, A.; *et al. In Situ* Observation of the Electrochemical Lithiation of a Single SnO$_2$ Nanowire Electrode. *Science* **2010**, *330*, 1515–1520.

41. Zhang, L. Q.; Liu, X. H.; Liu, Y.; Huang, S.; Zhu, T.; Gui, L.; Mao, S. X.; Ye, Z. Z.; Wang, C. M.; Sullivan, J. P.; *et al.* Controlling the Lithiation-Induced Strain and Charging Rate in Nanowire Electrodes by Coating. *ACS Nano* **2011**, *5*, 4800–4809.

42. Meunier, V.; Kephart, J.; Roland, C.; Bernholc, J. *Ab Initio* Investigations of Lithium Diffusion in Carbon Nanotube Systems. *Phys. Rev. Lett.* **2002**, *88*, 075506-1–4.

43. Yang, Z.-H.; Wu, H.-Q. Electrochemical Intercalation of Lithium into Carbon Nanotubes. *Solid State Ionics* **2001**, *143*, 173–180.

44. Peng, B.; Locascio, M.; Zapol, P.; Li, S.; Mielke, S. L.; Schatz, G. C.; Espinosa, H. D. Measurements of Near-Ultimate Strength for Multiwalled Carbon Nanotubes and Irradiation-Induced Crosslinking Improvements. *Nat. Nanotechnol.* **2008**, *3*, 626–631.

45. Kis, A.; Csányi, G.; Salvetat, J. P.; Lee, T.-N.; Couteau, E.; Kulik, A. J.; Benoit, W.; Brugger, J.; Forró, L. Reinforcement of Single-Walled Carbon Nanotube Bundles by Intertube Bridging. *Nat. Mater.* **2004**, *3*, 153–157.

46. Sammalkorpi, M.; Krasheninnikov, A. V.; Kuronen, A.; Nordlund, K.; Kaski, K. Irradiation-Induced Stiffening of Carbon Nanotube Bundles. *Nucl. Instrum. Methods Phys. Res., Sect. B* **2005**, *228*, 142–145.

47. Huhtala, M.; Krasheninnikov, A. V.; Aittoniemi, J.; Stuart, S. J.; Nordlund, K.; Kaski, K. Improved Mechanical Load Transfer between Shells of Multiwalled Carbon Nanotubes. *Phys. Rev. B* **2004**, *70*, 045404-1–8.

48. Sammalkorpi, M.; Krasheninnikov, A.; Kuronen, A.; Nordlund, K.; Kaski, K. Mechanical Properties of Carbon Nanotubes with Vacancies and Related Defects. *Phys. Rev. B* **2004**, *70*, 245416-1–8.

49. Dewar, M. J. S.; Zoebisch, E. G.; Healy, E. F.; Stewart, J. J. P. The Development and Use of Quantum Mechanical Molecular Models. 76. AM1: A New General Purpose Quantum Mechanical Molecular Model. *J. Am. Chem. Soc.* **1985**, *107*, 3902–3909.

50. Persson, K.; Hinuma, Y.; Meng, Y. S.; Van der Ven, A.; Ceder, G. Thermodynamic and Kinetic Properties of the Li-Graphite System from First-Principles Calculations. *Phys. Rev. B* **2010**, *82*, 125416-1–9.

51. Qi, Y.; Harris, S. J. *In Situ* Observation of Strains during Lithiation of a Graphite Electrode. *J. Electrochem. Soc.* **2010**, *157*, A741–A747.

52. Boudaoud, A.; Patricio, P.; Couder, Y.; Ben Amar, M. Dynamics of Singularities in a Constrained Elastic Plate. *Nature* **2000**, *407*, 718–720.

53. Vaziri, A.; Mahadevan, L. Localized and Extended Deformations of Elastic Shells. *Proc. Natl. Acad. Sci. U.S.A.* **2008**, *105*, 7913–7918.

54. Cottrell, A. H. *Concepts of the Electron Theory of Aollys*; IOM Communications Ltd.: London, 1998.

55. Jokl, M. L.; Vitek, V.; McMahon, C. J. A Microscopic Theory of Brittle Fracture in Deformable Solids: A Relation between Ideal Work to Fracture and Plastic Work. *Acta Metall.* **1980**, *28*, 1479–1488.

56. Nardelli, M. B.; Yakobson, B. I.; Bernholc, J. Brittle and Ductile Behavior in Carbon Nanotubes. *Phys. Rev. Lett.* **1998**, *81*, 4656–4659.